Journal of Global Positioning Systems (2026)
Vol. 22, Issue 1: 114-125
DOI:10.5081/jgps.22.1.114

Comparative analysis of carrier-phase level FDE for GF and GB models in urban multipath environments

Qi Cheng*, Wu Chen

Department of Land Surveying and Geospatial Science, the Hong Kong Polytechnic University, Hong Kong, China

Correspondence: Qi Cheng, qi001.cheng@connect.polyu.hk

Abstract: The increasing demand for centimeter-level positioning in autonomous driving and urban air mobility is frequently hindered by multipath (MP) and non-line-of-sight (NLOS) signals in urban canyons. While fault detection and exclusion (FDE) is essential for ambiguity resolution, traditional code-phase level FDE suffers from low sensitivity due to the similar magnitudes of observation noise and multipath-induced faults. In contrast, carrier-phase level FDE offers significantly higher sensitivity, as carrier-phase noise is orders of magnitude smaller than the biases introduced by incorrect integer cycles. This paper provides a rigorous theoretical analysis comparing two primary ambiguity resolution models for carrier-phase level FDE: the geometry-free (GF) model and the geometry-based (GB) model. We demonstrate the specific advantages of the GF model for FDE in urban environments, particularly its ability to isolate incorrectly resolved ambiguities independent of the receiver-satellite geometry. To validate the theoretical findings, vehicular experiments were conducted in the challenging urban environments of Nanjing and Hong Kong. The performance of a GF-based FDE real-time kinematic (RTK) algorithm was compared with the post-processed kinematic (PPK) of an industry-leading commercial software, Leica Infinity. Experimental results indicate that the GF-FDE RTK algorithm demonstrates superior robustness, achieving higher ambiguity fix rates and comparable positioning accuracy compared to the commercial benchmark in harsh urban environments. The findings highlight the significant potential of GF-based carrier-phase FDE to enhance the availability and reliability of high-precision navigation engines.

Keywords: GNSS, Carrier Phase, GF Model, Urban Canyon, FDE

I. Introduction

The demand for centimeter-level positioning in urban environments has surged with the advent of autonomous driving and urban air mobility. While Global Navigation Satellite Systems (GNSS) are the primary source of positioning, urban canyons pose a significant challenge due to Multipath (MP) and Non-Line-of-Sight (NLOS) signals (Hsu 2017; Suzuki et al 2020; Xu et al 2024). These errors can introduce significant positioning biases ranging from several to tens of meters, making Fault Detection and Exclusion (FDE) essential to ensure the high-precision positioning of the navigation system (Chen et al 2023; Sun et al 2021).

Traditionally, FDE mechanisms have been implemented at the code-phase (pseudorange) level (Hwang et al 2006; Parkinson and Axelrad 1988; Zhang and Papadimitratos 2021). However, the effectiveness of code-based FDE is severely limited in urban environments. The fundamental issue is that code-phase noise and multipath-induced faults are often of the same order of magnitude. This statistical similarity makes it difficult to distinguish a genuine fault from inherent observation noise, leading to high missed detection rates. In addition, evaluating only the code-phase is insufficient to truly reflect the quality of carrier-phase measurements, which has a greater impact on ambiguity resolution. Consequently, code-based FDE lacks the sensitivity required to protect high-precision applications from subtle but critical errors.

To overcome this limitation, carrier-phase level FDE is employed. The carrier-phase observation noise is relatively low (at the millimeter to centimeter level) (Wu et al 2025). An incorrectly fixed ambiguity typically introduces a bias of at least approximately 20 cm (corresponding to the carrier wavelength and incorrect cycles), which is an order of magnitude larger than the carrier-phase noise. However, prior to the execution of carrier-phase FDE, the integer ambiguities should first be resolved. Common ambiguity resolution methods can be broadly categorized into Geometry-Free (GF) and Geometry-Based (GB) models (Teunissen et al 2002).

Existing carrier-phase integrity monitoring or FDE frameworks rely mainly on the GB model. The GB model exploits spatial redundancy and geometric constraints across the entire constellation to estimate parameters (Teunissen et al 2002). However, this global spatial coupling introduces a critical drawback for integrity monitoring. Because all integer ambiguities are jointly estimated within a unified functional model, an uncorrected gross error on a single satellite is mathematically distributed across the entire ambiguity vector. Consequently, the resulting carrier-phase residuals become insensitive to localized faults, making FDE exceedingly difficult.

In contrast, the GF model eliminates geometric range parameters from individual satellite-pair, enabling integer ambiguities to be resolved independently per satellite-pair (Teunissen et al 2002). Because the ambiguity resolution is decoupled across satellites, an uncorrected gross error does not contaminate other satellite ambiguity resolution. This decoupling ensures that any ambiguity fixing error manifests as a sharp, highly prominent spike in the post-fix carrier-phase residuals, conferring superior fault sensitivity and separability compared to GB models.

Despite these theoretical differences, a clear comparative analysis of post-fix carrier-phase residual behavior and FDE sensitivity between GF and GB models deserves investigation, particularly in challenging urban areas. To address this gap, this paper provides a rigorous theoretical and experimental investigation into the post-fix error propagation of GF and GB frameworks.

The main contributions of this paper are summarized as follows:

1. We theoretically analyzed the sensitivity of post-fit carrier-phase residuals to incorrectly fixed ambiguities under both GB and GF models. This demonstrates the superior effectiveness and higher sensitivity of the GF-based FDE model, which was further confirmed by empirical residual analysis.
2. We validated the proposed GF FDE framework using real-world multi-frequency GNSS datasets collected across various challenging urban scenarios. The experimental results demonstrate that the proposed method significantly outperforms commercial benchmark software (Leica Infinity) in both ambiguity fix rate and reliability.

II. Methodology

A. GF and GB models

Taking GPS L1 as an example, we briefly introduce the GF and GB models in a short baseline here. The double-differenced code and carrier-phase measurements are as follows (Teunissen and Montenbruck 2017):

$$P^{ij} = r^{ij} + \varepsilon^{ij} \quad (1)$$

$$L^{ij} = r^{ij} + \lambda N^{ij} + \epsilon^{ij} \quad (2)$$

where i and j denote satellites; P is the code-phase; L is the carrier-phase in meters; r is the geometrical range; λ is the wavelength; N is the integer ambiguity; ε and ϵ are noise of code and carrier-phase. The atmospheric errors are ignored.

In the GF model, the ambiguity can be directly resolved by code-phase directly:

$$N^{ij} = round(\frac{L^{ij} - P^{ij}}{\lambda}) \quad (3)$$

where, $round(\quad)$ means rounding operation. It should be noted that the success rate is low of GF model using only one frequency. Using multi-frequency can significantly increase this rate, such as three-carrier ambiguity resolution (TCAR) (Feng 2008).

When there are n double-differenced satellite-pairs, we have:

$$y = Aa + Bb + \xi \quad (4)$$

where, A and B are designed matrices; a is the integer ambiguity vector and b is the position correction vector; y contains double-differenced code and carrier-phase measurements, and ξ contains random noise.

In the GB model, to solve the integer ambiguities, the goal is to minimize the following value function (Teunissen and Montenbruck 2017):

$$C_W(a,b) = (y - Aa - Bb)^T Q^{-1} (y - Aa - Bb). \quad (5)$$

where, Q is the variance-covariance matrix of y.

The estimations of a and b can be decomposed into three steps (Teunissen 1995). In the first step, the integer property of a is disregarded, and the float solution $\hat{a}$ and $\hat{b}$ can be computed via weighted least-squares (Teunissen and Montenbruck 2017):

$$\begin{bmatrix} \hat{a} \\ \hat{b} \end{bmatrix} = \left(\begin{bmatrix} A^T \\ B^T \end{bmatrix} Q^{-1} [A \quad B] \right)^{-1} \begin{bmatrix} A^T \\ B^T \end{bmatrix} Q^{-1} y. \quad (6)$$

The corresponding variance-covariance matrix can be calculated as follows (Teunissen and Amiri-Simkooei 2008):

$$\begin{bmatrix} Q_{\hat{a}} & Q_{\hat{a}\hat{b}} \\ Q_{\hat{b}\hat{a}} & Q_{\hat{b}} \end{bmatrix} = ([A \quad B]^T Q^{-1} [A \quad B])^{-1}. \quad (7)$$

Minimizing equation (5) is equal to minimizing the following value function, which was proven by Teunissen (1995):

$$C(a) = (a - \hat{a})^T Q_{\hat{a}}^{-1} (a - \hat{a}). \qquad (8)$$

Therefore, the two models can both obtain integer ambiguity candidate vector.

B. Potential benefits of GF model to GB model in FDE

In this section, we theoretically analyze the differences in the FDE process after ambiguity resolution when using the GB and GF models, respectively.

We assume that the only carrier-phase observation equations in a short baseline can be expressed as:

$$y_1 = A_1 a + B_1 b + \xi_1 \qquad (9)$$

where, y_1 denotes the only carrier-phase observation vector; A_1 and B_1 are the design matrices; ξ_1 is the carrier-phase noise vector. Once the integer ambiguities have been resolved using the GB or GF models, the carrier-phase observation equation becomes:

$$y_1 - A_1 N_{True} = B_1 b + e + \xi_1 \qquad (10)$$

where, $e = A_1 \Delta N$. ΔN is the difference between the resolved ambiguity vector and the true ambiguity vector:

$$\Delta N = N_{resolved} - N_{True}. \qquad (11)$$

If the resolved ambiguities correspond to the true values, all elements in ΔN will be zero:

$$\Delta N = [0 \quad 0 \quad 0 \quad \dots \quad 0 \quad 0 \quad 0]_n^T. \qquad (12)$$

Then, the corresponding positioning error after ambiguity resolution in this case is (Teunissen and Montenbruck 2017):

$$\Delta b = -(B_1^T W B_1)^{-1} B_1^T W \xi_1 \qquad (13)$$

where, $W = Q_1^{-1}$ is the weight matrix for the carrier-phase observation equation; Q_1 is the variance-covariance matrix of carrier-phase vector. Δb is positioning error. In this case, the positioning error is influenced only by the carrier-phase noise and the satellite geometric configuration. The typical positioning accuracy can reach centimeter level. The residual vector at this stage is (Teunissen and Montenbruck 2017):

$$v = -M\xi_1 \qquad (14)$$

where, $M = I - B_1(B_1^T W B_1)^{-1} B_1^T W$, and I is the identity matrix. Since ξ_1 represents the carrier-phase noise, the residual vector is typically very small if all resolved ambiguities are correct. Consequently, the commonly used test statistics, post-fit sum of squared carrier-phase residuals ($v^T W v$), will also be small, and the solution will generally pass detection algorithms based on residual analysis, such as the Chi-square test.

Let $P = B_1(B_1^T W B_1)^{-1} B_1^T W$ be the projection matrix onto the parameter subspace, and $M = I - P$ the projection matrix onto the residual subspace. According to the projection decomposition theorem in linear algebra (Strang 2022), the following relationship holds:

$$\|\xi_1\|_W^2 = \|P\xi_1\|_W^2 + \|M\xi_1\|_W^2 \qquad (15)$$

where, $\| \ \|_W^2$ denotes the squared weighted Euclidean norm, i.e., $\|x\|_W^2 = x^T W x$. Specifically, $\|\xi_1\|_W^2$ is the total weighted sum of squares (TSS) of the observation noise. $\|P\xi_1\|_W^2$ is the weighted explained sum of squares (ESS), reflecting the precision of the estimated parameters, and $\|M\xi_1\|_W^2$ is the weighted post-fit residual sum of squares (RSS). This formula demonstrates that the observation noise is distributed onto the parameter subspace and the residual subspace by the respective projection matrices.

If the resolved ambiguities are incorrect, ΔN actually represents the ambiguity errors, and its elements are all integers. In the GF model, the ambiguities in each equation are fixed independently, and most of them can be correctly resolved (if using TCAR). The TCAR correct rates can be more than 80% in urban areas, using a short baseline (Cheng et al., 2024). Suppose there are n double-differenced equations, and l ambiguities are incorrectly resolved. In this case, ΔN is:

$$\Delta N = [0 \quad 0 \quad k1 \quad \dots \quad kl \quad \dots \quad 0 \quad 0 \quad 0]_n^T \qquad (16)$$

where, $k1$ to kl are all integers. The corresponding position error and the residual vector in this case are:

$$\Delta b = -(B_1^T W B_1)^{-1} B_1^T W (e + \xi_1) \qquad (17)$$

$$v = -M(e + \xi_1). \qquad (18)$$

Since $M^2 = M$ and $(WM)^T = WM$, the $v^T W v$ can be simplified as:

$$v^T W v = (e + \xi_1)^T W M (e + \xi_1). \qquad (19)$$

According to equation (19), to achieve effective FDE, $v^T W v$ should become much larger if e is not the zero vector. Therefore, two requirements should be met:

1) e should be much larger than the noise ξ_1;
2) e should not be orthogonal to the column space of the projection matrix M, i.e. $Me \neq \mathbf{0}$.

For the carrier-phase based FDE using GB model, requirement 2 cannot be met, where Me is very small, close to zero vector. In the GB model, the elements of e are no longer independent, nor are they independent of the satellite geometry matrix B_1. In fact, under the influence of the projection matrix M, e is projected in such a way that the minimum possible squared norm remains in the residual subspace.

Let us revisit equation (5), which essentially serves as the ambiguity resolution criterion for the GB model. In other words, the solution found by the GB model is guaranteed to minimize the sum of squared residuals in this equation, based on the integer least-squares principle. Since using only the carrier-phase equations would make equation (5) rank-deficient, it is common practice to use both code and carrier-phase observations together, so that the RSS of code and carrier-phase is minimized. In equation (5), the noise standard deviation of the code-phase observations is often set to be 100 times larger than that of the carrier-phase observations. As a result, the carrier-phase RSS dominates the overall residual sum. When the total RSS in equation (5) is minimized, the post-fit carrier-phase RSS is also close to its minimum value in equation (9).

Therefore, even if the ambiguities resolved by the GB model are incorrect, most of the errors in the ambiguities will be projected onto the parameter subspace, with only a small portion being projected onto the residual subspace. As a result, the post-fit carrier-phase RSS remains at a low level, making further FDE challenging.

When using traditional code-phase based FDE, the bias (multipath error, not incorrect ambiguities) may be similar in magnitude to the noise, especially in urban environments. In this case, requirement 1 cannot be satisfied. When the bias is indistinguishable from the noise, it becomes difficult to reliably detect and exclude faulty measurements, thereby reducing the effectiveness of the FDE process.

As for the GF model, negligible multipath errors do not affect ambiguity resolution and are typically treated as stochastic noise. In contrast, significant multipath and NLOS errors can lead to incorrect ambiguity fixes, being magnified during the integer estimation process. This will benefit the FDE algorithms.

In addition, from both algebraic and geometric perspectives, the error vector e from GF model introduced exhibits strong discrete randomness. Since ambiguity resolution processes are independent, the erroneous integer sequence $k1$ to kl is algebraically uncorrelated with the satellite geometry design matrix B_1. For the error vector e to be absorbed in the residual subspace, it must reside within the column space of B_1, meaning that the n-dimensional observation error e would need to be fully explained by a 3-dimensional coordinate shift Δb. However, under the constraints of complex multi-constellation geometry, and given the lack of correlation between e and B_1, the probability that a random integer error vector aligns with this low-dimensional physical subspace is exceedingly small. Since the error vector e is generated independently of the satellite geometry matrix B_1, the direction of e can be regarded as isotropic in the n-dimensional observation space. According to the properties of orthogonal projection, the expected value of the squared norm of the vector e projected onto the residual subspace of dimension $n-m$ is determined by the ratio of the dimension of this subspace to that of the entire space (Strang 2012). If the ambiguity vector is incorrect, the e is much larger than noise ξ_1, and will result in a significant increase in v^TWv within the residual subspace. Consequently, ambiguities resolved by the GF model are inherently well-suited for post-fit FDE process.

C. Case study

Here, we use one epoch GPS L1 data in a short baseline to validate the previous theoretical analysis. At this epoch, there are ten satellites, and the double-differenced design matrix B_1 and double-differenced carrier-phase (m) is shown in table I. The carrier-phase noise is set as follows (Li et al 2022):

$$\sigma_L^2 = 0.003^2 \times (1 + \frac{1}{\sin(\theta)})^2 \qquad (20)$$

where, θ is elevation angle. Since $W = Q_1^{-1}$, the weighting matrix W for the carrier-phase observations can be computed as table II.

At this point, the correct ambiguity vector is N_{true} = [-90 -2 3 39 20 141 5 1 -14]^T. When the ambiguities are correctly resolved, the positioning error (in meters) is: Δb = [-0.0006 0.0045 0.0013]. The carrier-phase residual vector (in meters) is: v =[-0.0037 0.0027

-0.0066 -0.0039 -0.0001 0.0006 0.0004 0.0020 -

0.0006].

The sum of squared residuals is 0.21. This result confirms that, when the ambiguities are correctly resolved, the post-fit sum of squared carrier-phase residuals remains small.

When using the GB model for ambiguity resolution, the Least-squares AMBiguity Decorrelation Adjustment (LAMBDA) algorithm is applied as an example (Teunissen 1995). To ensure that the optimal solution found by the LAMBDA algorithm corresponds to an incorrect ambiguity, a gross error of 10 meters was introduced to the code-phase in the third equation. No additional error was added to the carrier-phase observations. The error vector of the optimal solution found by the LAMBDA search is: ΔN = [25 -22 -11 -2 21 -4 -7 17 -24]^T. The estimated positioning error (in meters) in this case is: Δb = [-2.7203 -3.6416 -2.6664]. The corresponding residual vector (in meters) is:

$v =$[0.0091 -0.0125 -0.0139 -0.0051 0.0004 -0.0012 -0.0076 -0.0089 0.0093].

Table I. Design matrix B_1 and double-differenced carrier-phase of GPS at an epoch

Satellite-pair	$(I_i - I_{pivot})_x$	$(I_i - I_{pivot})_y$	$(I_i - I_{pivot})_z$	DD carrier-phase (m)
1	-0.0090	1.2438	0.0734	-17.124
2	-0.5974	-0.3265	-0.5562	-0.380
3	0.1966	0.1598	-1.2172	0.563
4	-0.4351	0.0645	0.1870	7.418
5	0.4241	0.8690	-0.1442	3.809
6	-0.9507	0.3535	0.1800	26.834
7	0.3195	0.1472	-1.0386	0.951
8	0.1709	0.6205	0.1797	0.195
9	-0.3525	-0.2471	-1.0372	-2.667

Table II The weighting matrix W for the carrier-phase observations

156.2	-22.3	-6.2	-27.2	-10.7	-12.2	-11.6	-20.7	-14.2
-22.3	4227.5	-194.5	-855.4	-337.2	-383.5	-362.9	-649.0	-445.9
-6.2	-194.5	1315.9	-237.9	-93.8	-106.6	-100.9	-180.5	-124.0
-27.2	-855.4	-237.9	4978.0	-412.3	-468.8	-443.7	-793.4	-545.2
-10.7	-337.2	-93.8	-412.3	2212.1	-184.8	-174.9	-312.8	-214.9
-12.2	-383.5	-106.6	-468.8	-184.8	2490.2	-198.9	-355.7	-244.4
-11.6	-362.9	-100.9	-443.7	-174.9	-198.9	2367.3	-336.6	-231.3
-20.7	-649.0	-180.5	-793.4	-312.8	-355.7	-336.6	3968.2	-413.6
-14.2	-445.9	-124.0	-545.2	-214.9	-233.4	-231.3	-413.6	2856.0

The post-fit sum of squared carrier-phase residuals is 1.40. When using the GB model, even if the ambiguity is incorrectly fixed, the sum of carrier-phase residuals remains small, making FDE difficult. In contrast, the positioning error becomes very large. This confirms our previous analysis: in the GB model, the overall integer least-squares solution minimizes the sum of squared residuals as much as possible, and the incorrect ambiguity vector is mostly projected onto the parameter space.

When using the GF model to resolve ambiguities, the resolution process for different ambiguities is independent. Suppose the third ambiguity is incorrectly fixed by one cycle, while all other ambiguities are correctly fixed. Although the success rate for single-frequency GF models may not reach this level, it is entirely possible in three-frequency scenarios. In this case, the error ambiguity vector is: $\Delta N = [0\ 0\ 1\ 0\ 0\ 0\ 0\ 0\ 0]^T$. Similarly, we can compute the positioning error (in meters) as follows:$\Delta b =$ [-0.0002 -0.0213 0.0409].

The corresponding residual vector (in meters) is: $v =$[0.0273 0.0159 0.0460 -0.0097 0.0273 0.0030 0.0456 0.0105 0.0335].

The sum of squared residuals in this case is 10.62. It can be seen that, even though only one ambiguity is incorrectly resolved by one cycle in the GF model, the sum of squared carrier-phase residuals increases significantly. This is advantageous for subsequent FDE. The positioning error also increases slightly, which is consistent with our previous analysis: the incorrectly resolved ambiguity vector is proportionally projected onto both the parameter space and the residual space. However, although the sum of squared residuals increases substantially, it is unfortunate that the error in the third ambiguity not only causes the third residual to increase, but also leads to increases in other residuals to some extent. This indicates that further research is needed to achieve effective FDE.

A triple-frequency experiment collected in an urban canyon environment in Hong Kong was utilized to further validate this conclusion. BDS-2 and Galileo observations sampled at 1 Hz were processed. Fig. 1 illustrates the performance of the GB LAMBDA, presenting both the positioning solutions and the sum of squared carrier-phase residuals for correctly and incorrectly estimated ambiguities. In line with our previous theoretical analysis, under the GB model, the impact of incorrectly fixed ambiguities is absorbed predominantly by the parameter space, with only a minor fraction projected onto the residual space. Consequently, the carrier-phase RSS shows no significant amplification during false-fix epochs.

Fig. 2 depicts the performance using the same dataset processed by the GF TCAR model. In contrast, under the GF model, false fixes are significantly projected onto both the parameter and residual spaces, leading to a dramatic spike in the carrier-phase RSS during false-fix epochs. This distinct residual signature renders the GF TCAR model suitable for subsequent FDE. Although the GB LAMBDA exhibits a slightly higher fix rate, the GF TCAR complemented by an effective FDE mechanism holds potential to yield superior positioning performance in challenging urban environments.

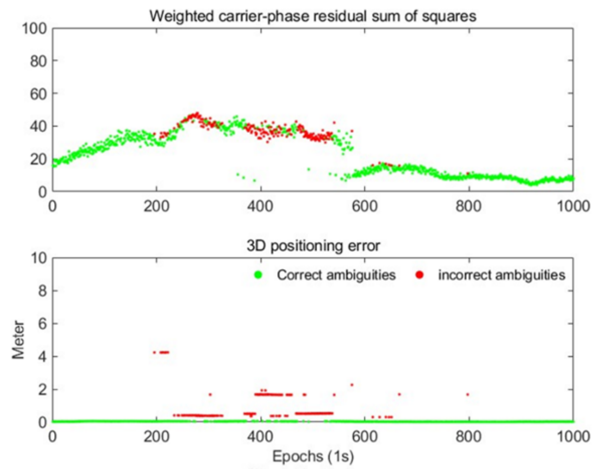

Fig. 1. Performance of GB LAMBDA estimated integer ambiguities: (bottom) 3D positioning error and (top) weighted carrier-phase residual sum of squares.

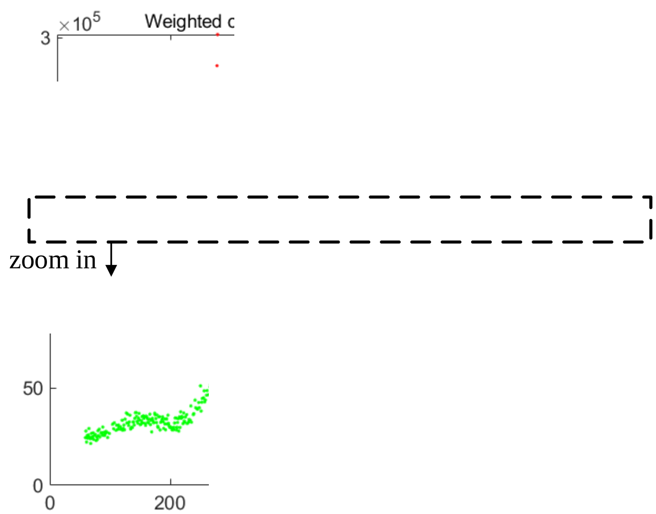

Fig. 2. Performance of GF TCAR estimated integer ambiguities: (bottom) 3D positioning error and (top) weighted carrier-phase residual sum of squares

III. Experiments

Based on the above analysis, almost all traditional FDE algorithms can achieve satisfactory performance at the carrier-phase level when using the GF model. A representative example is our previous work, the random sample consensus (RANSAC) based TCAR method (Cheng et al., 2024). In this section, we compare the previously proposed RTK algorithm with the commercial post-processed kinematic (PPK) software, Leica Infinity 4.1.3, a version officially recognized for its enhanced ambiguity resolution capabilities in severe multipath environments (Leica Geosystems, 2024).

The first vehicular experiment was conducted in a typical urban environment in Nanjing over a one-hour period with a sampling rate of 1 Hz. Triple-frequency observations from BDS (BDS-2 and BDS-3), GPS, and Galileo were utilized. The reference trajectory was generated using a high-grade Inertial Measurement Unit (IMU), the Honeywell HGuide N580, combined with a GNSS/INS integrated solution from Inertial Explorer (IE) in RTK mode. More details regarding the experimental setup can be found in Cheng et al. (2024).

To ensure a fair comparison, identical satellite constellations and frequency bands were utilized for both algorithms. Table III summarizes the ambiguity resolution performance of the proposed RTK algorithm and Leica PPK. The proposed method achieved 2,630 fixed epochs, notably higher than the 2,083 epochs recorded by Leica PPK. Regarding positioning accuracy, the proposed RTK outperformed Leica PPK, with 2,074 epochs maintaining a 3D error below 10 cm, compared to only 1,119 epochs for the latter. Furthermore, the proposed RTK yielded a 3D RMSE of 20.35 cm, representing an improvement over Leica PPK's 26.44 cm. The corresponding positioning error time series and distributions are illustrated in Figs 3 and 4, respectively.

Table III. Epochs of 3D positional errors less than 10 cm, maximum error, RMSE, fixed epochs in Nanjing

Methods	<10 cm (epoch)	Max (cm)	RMSE (cm)	Fixed epochs
Proposed RTK	2074	120.10	20.35	2630
Leica PPK	1119	120.43	26.44	2083

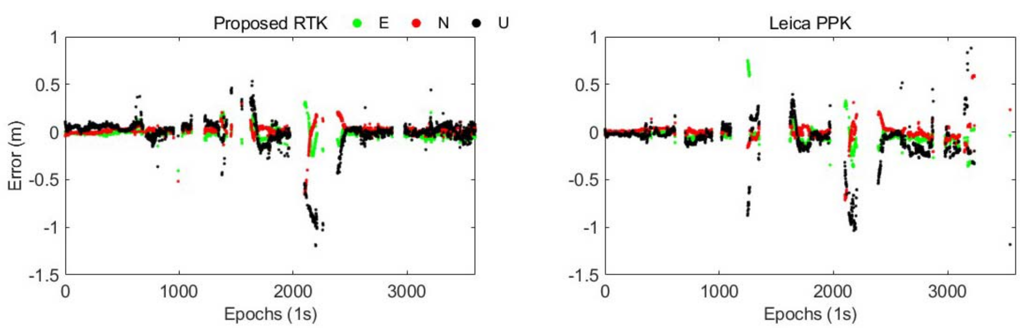

Fig. 3. Positioning errors of vehicular experiment in Nanjing

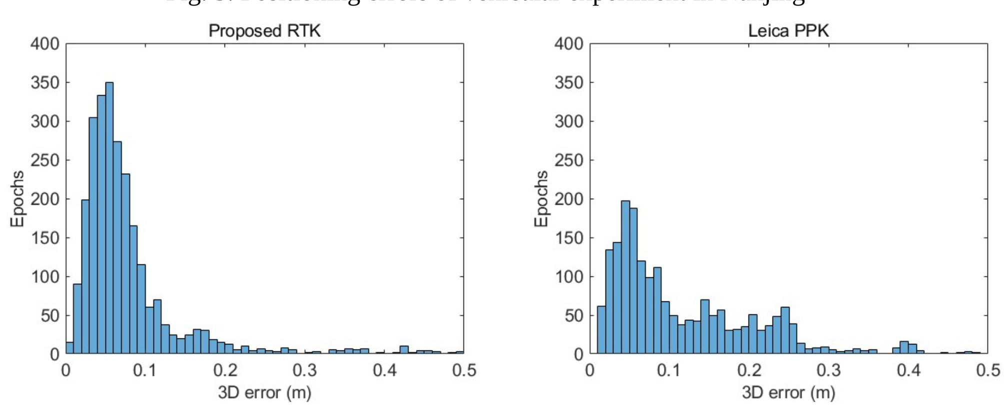

Fig. 4. 3D positioning error distributions in Nanjing

To further validate the GF-FDE model, a specialized RTK software was developed based on the algorithm proposed in Cheng et al. (2024). This software supports GF models for three, four and five-frequency observations, depending on the available frequency bands. A second vehicular experiment was conducted in the more challenging urban environment of Hong Kong (see table IV for experimental settings). Again, identical satellite constellations and frequency bands were utilized for both algorithms. As illustrated in Fig. 5, the number of available satellites fluctuated rapidly due to frequent signal blockages in the complex urban landscape. Despite utilizing three constellations, satellite availability remained insufficient for positioning in numerous epochs. The experimental environment, shown in Fig. 6, is characterized by frequent GNSS signal obstruction and reflection, which lead to significant NLOS and multipath errors.

Table IV. The details of the experimental setting in Hong Kong

Base station	Antenna: Leica AR25.R4+LEIT; Receiver: Leica GR50			
Rover station	Antenna: Harxon GPS320; Receiver: SEPT POLARX5E			
Baseline	3.2-5.7 km			
Sampling duration	About 2 h			
Sampling rate	1 Hz			
Constellation	BDS-2	BDS-3	Galileo	GPS
Carrier frequency	B1 B2 B3	B1 B1C B2a B3	E1 E5a E5b E5 E6	L1, L2, L5

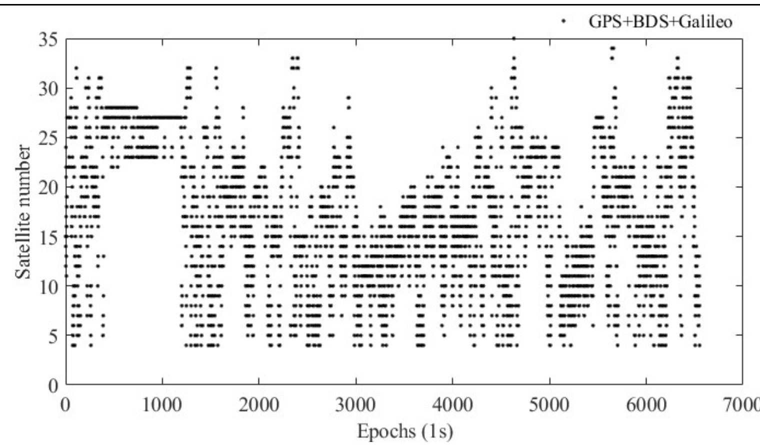

Fig. 5. Number of available satellites in Hong Kong

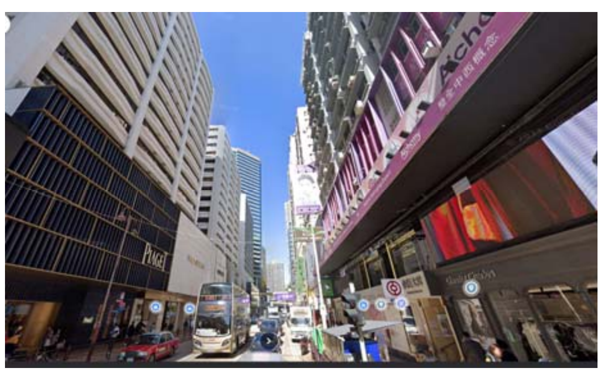
Fig. 6. Experiment environments in Hong Kong

Owing to the extreme harsh urban conditions, a reliable reference trajectory was unavailable for this experiment. Consequently, the performance evaluation primarily focuses on the ambiguity fix rates. As summarized in table V and Fig. 7, the developed RTK software achieved a fix rate of 61.1%, nearly doubling the 30.6% recorded by Leica PPK. This significant disparity is further illustrated in Figs 8 and 9, which present the estimated trajectories with magnified insets for closer inspection. The visual evidence in the magnified insets suggests that the developed RTK software effectively suppresses the impact of NLOS and multipath interference, providing fixed solutions, whereas the commercial software struggles to do so. These results demonstrate the robustness and superior reliability of the GF-model-based carrier-phase FDE, highlighting its significant potential for high-precision positioning in challenging GNSS environments.

It should be acknowledged as a practical limitation that the performance assessment in this experiment relies primarily on the ambiguity fix rate due to the unavailability of a continuous high-precision reference trajectory. Nevertheless, as demonstrated in the preceding Nanjing experiment under controlled conditions, the proposed algorithm achieved improvements in both fix rate and 3D positioning accuracy (RMSE). Given that similar algorithms were used across both experiments, it can be reasonably inferred that the higher fix rate in the Hong Kong scenario reflects reliable ambiguity resolution without compromising positioning precision.

Table V. Epochs of fixed solutions for two algorithms in Hong Kong

Methods	Fixed epochs
Developed RTK	4003
Leica PPK	2003

IV. Conclusions

In this study, we have investigated the implementation of FDE at the carrier-phase level, specifically focusing on the advantages of the GF model. By decoupling the incorrect

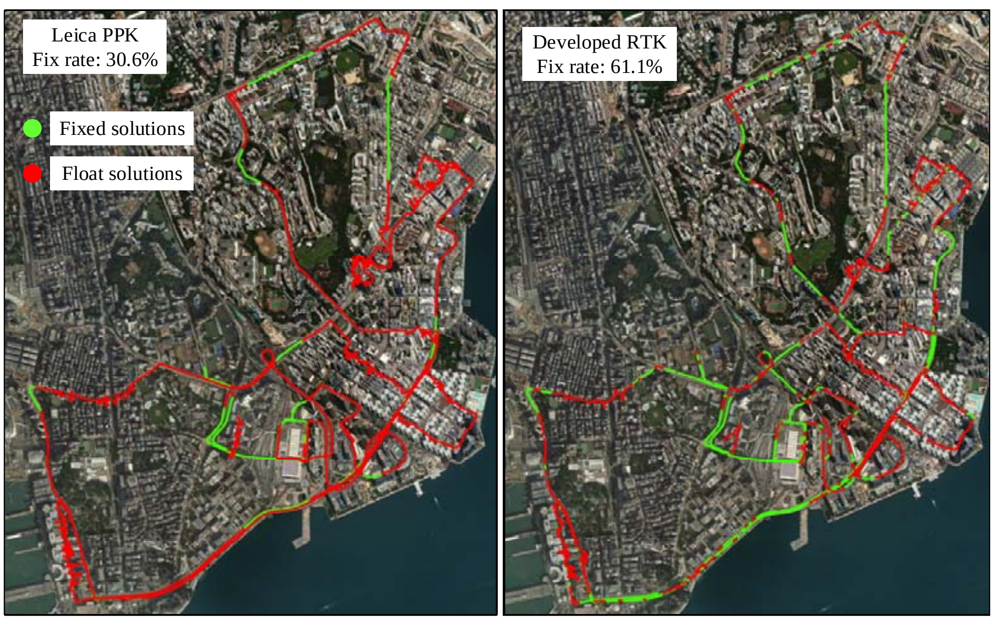

Fig. 7. Trajectories and fix rates of the two methods in Hong Kong

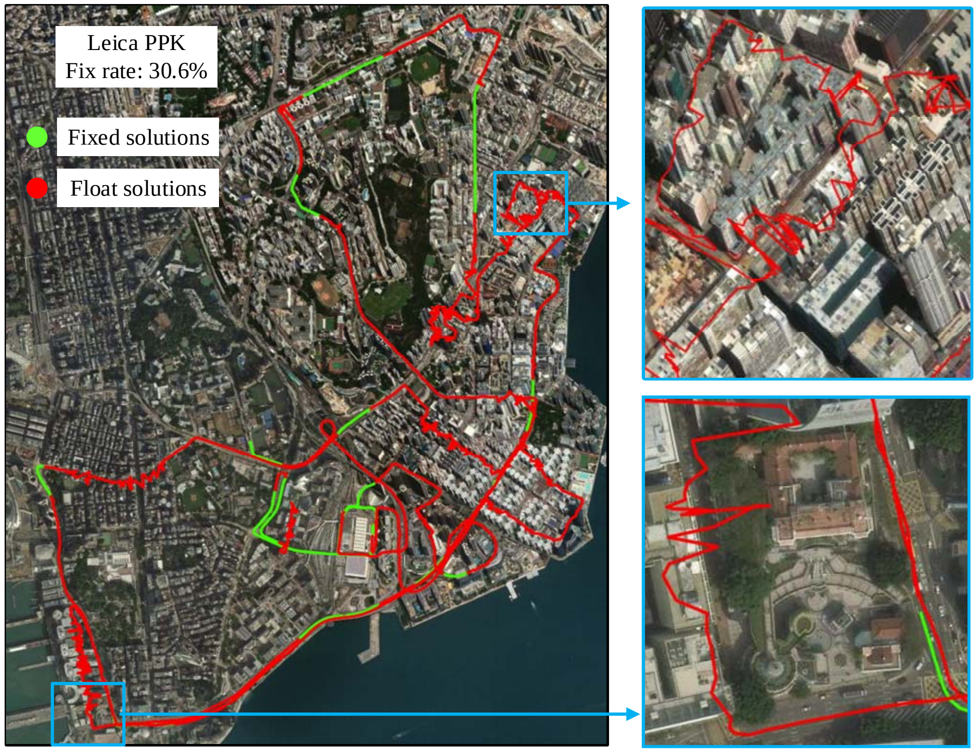

Fig. 8. Trajectory of the Leica PPK results with magnified insets in Hong Kong

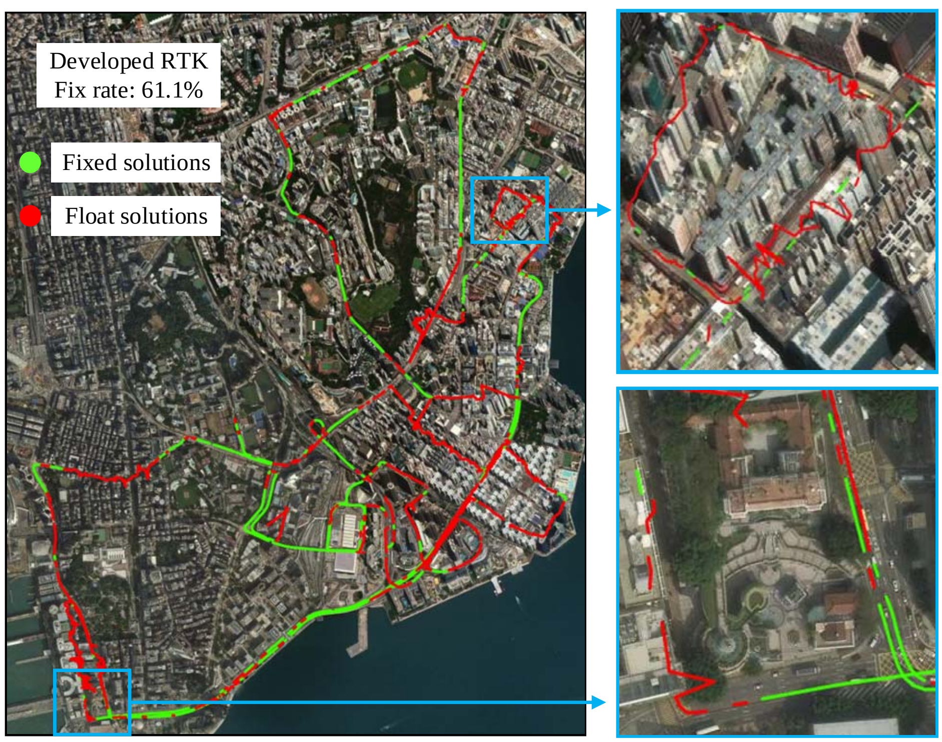

Fig. 9. Trajectory of the developed RTK results with magnified insets in Hong Kong

ambiguities from the satellite-receiver geometry, the GF-based FDE demonstrates superior robustness in identifying and isolating individual satellite anomalies, compared to the traditional GB model.

The experimental validation involved comparison between our previous proposed GF-FDE based RTK algorithm and the industry-leading Leica PPK commercial software. The results indicate that the proposed algorithm exhibits a competitive performance, maintaining high positioning accuracy and fix rate in harsh urban environments. Notably, the developed RTK software demonstrates certain advantages over the Leica PPK in terms of integer ambiguity fix rate. These findings underscore the significant potential of carrier-phase level FDE algorithms using the GF model for high-precision GNSS applications.

Declarations

Ethics approval and consent to participate

Not applicable.

Availability of data and materials

The data that support the results of this study are available from the corresponding author for academic purposes on reasonable request.

Competing interests

The authors declare no conflict of interest.

Funding

The authors are grateful for the sponsorship of the Hong Kong General Research Fund (Grant No. 15229622), Guangdong - Hong Kong Technology Cooperation Funding Scheme (Grant No. GHP/033/22SZ), and Shenzhen Science and Technology Program under Grant SGDX20230116092503007.

Authors' contributions

Qi Cheng conceived the idea, developed the theory, conducted the experiments and processed the data. All authors discussed the results and contributed to the final manuscript.

Acknowledgements

Many thanks for the people, who helped collecting data.

REFERENCES

Chen H, Sun R, Cheng Q and Yang L (2023). A factor set-based GNSS fault detection and exclusion for vehicle navigation in urban environments. GPS Solutions, 27(2), 87.

Cheng Q, Chen W, Sun R, Wang J and Weng D (2024). RANSAC-based instantaneous real-time kinematic positioning with GNSS triple-frequency signals in urban areas. Journal of geodesy, 98(4), 24.

Feng Y (2008). GNSS three carrier ambiguity resolution using ionosphere-reduced virtual signals. *Journal of geodesy*, 82(12), 847-862.

Hsu L T (2017, October). GNSS multipath detection using a machine learning approach. In 2017 IEEE 20th international conference on intelligent transportation systems (ITSC) (pp. 1-6). IEEE.

Hwang P Y and Brown R G (2006). RAIM-FDE Revisited: A New Breakthrough In Availability Performance With nioRAIM (Novel Integrity-Optimized RAIM). Navigation, 53(1), 41-51.

Leica Geosystems (2024). Leica Infinity v4.1.3 release notes. New Leica Infinity Release – v4.1.3 now available for download | Leica Geosystems.

Li Y, Zhang Z, He X, Yuan H and Zang N (2022). An elevation stochastic model constrained by C/N0 for GNSS real-time kinematic positioning in harsh environments. Measurement Science and Technology, 34(1), 015011.

Parkinson B W and Axelrad P (1988). Autonomous GPS integrity monitoring using the pseudorange residual. Navigation, 35(2), 255-274.

Strang G (2012). Linear algebra and its applications.

Strang G (2022). Introduction to linear algebra. Wellesley-Cambridge Press.

Sun R, Wang J, Cheng Q, Mao Y and Ochieng W Y (2021). A new IMU-aided multiple GNSS fault detection and exclusion algorithm for integrated navigation in urban environments. GPS Solutions, 25(4), 147.

Suzuki T, Matsuo K and Amano Y (2020). Rotating GNSS antennas: Simultaneous LOS and NLOS multipath mitigation. GPS Solutions, 24(3), 86.

Teunissen J G (1995). The least-squares ambiguity decorrelation adjustment: A method for fast GPS integer ambiguity estimation. Journal of Geodesy, 70, 65-82.

Teunissen P J and Amiri-Simkooei A R (2008). Least-squares variance component estimation. Journal of geodesy, 82, 65-82.

Teunissen P J and Montenbruck O (Eds.) (2017). Springer handbook of global navigation satellite systems (Vol. 10, pp. 978-3). Cham, Switzerland: Springer International Publishing.

Teunissen P, Joosten P and Tiberius C (2002, September). A comparison of TCAR, CIR and LAMBDA GNSS ambiguity resolution. In Proceedings of the 15th international technical meeting of the satellite division of the institute of navigation (ION GPS 2002) (pp. 2799-2808).

Wu Z, Yue Y and Wu M (2025). An improved carrier phase-based RAIM method applied to GNSS RTK positioning integrity for landslide monitoring. Advances in Space Research.

Xu P, Zhang G, Yang B and Hsu L T (2024). Machine learning in GNSS multipath/NLOS mitigation: Review and benchmark. IEEE Aerospace and Electronic Systems Magazine, 39(9), 26-44.

Zhang K and Papadimitratos P (2021). Fast multiple fault detection and exclusion (FM-FDE) algorithm for standalone GNSS receivers. IEEE Open Journal of the Communications Society, 2, 217-234

.

Authors

Qi Cheng received the bachelor's and master's degrees in transportation engineering from Nanjing University of Aeronautics and Astronautics, Nanjing, Jiangsu, China, in 2017 and 2021, respectively. He is currently pursuing the Ph.D. degree with the Department of Land Surveying and Geospatial Science, The Hong Kong Polytechnic University, Hong Kong. His research interest is GNSS high-precision positioning algorithms in urban areas.

Wu Chen received the Ph.D. degree from Newcastle University, Newcastle upon Tyne, U.K., in 1992. He is currently a Chair Professor of satellite navigation with the Department of Land Surveying and Geospatial Science, The Hong Kong Polytechnic University, Hong Kong. He has been actively working on global navigation satellite system (GNSS)-related research for more than 30 years. His main research interests include GNSS positioning quality evaluation, system integrity, various GNSS applications, seamless positioning, and simultaneous localization and mapping (SLAM).